ADVANCED MATERIALS TECHNOLOGIES
www.advmattechnol.de

Impact of Nanoparticle Size and Loading on Printability of Composite Inks for Direct Ink Writing

Yun Li, Aidan Flynn, Christopher Masternick, Brandon Kolanovic, Bin Li, and Bo Li**

Direct ink writing (DIW) using polymer-particle composite inks is a new research area enabling a wide range of new functionalities. Despite extensive studies, there remains a need for a deeper understanding of how particle size and loading specifically influence printability, especially in the nano range. This work aims to systematically evaluate the effects of SiO_2 nanoparticle size (26–847 nm) and loading on printability within a polydimethylsiloxane (PDMS) matrix. For the single-layer printing process, which is influenced by the substrate properties, a 3D printing line analysis (3D-PLA) is developed to monitor the top and side views of printed lines. It is found that line width varies with ink composition and substrate, while the line height decreases with solvent evaporation, indicating a strong confinement effect from the substrate. For multilayer structures, dual-layer printing analysis (DLPA) is utilized to evaluate the printability. It is shown that DLPA is independent of the substrate and can be used to compare the printabilities from different inks. Both 3D-PLA and DLPA can be correlated to the rheological behavior of the ink through ink rheology analysis (IRA). Finally, this research defined the design space for DIW by benchmarking the minimum and maximum particle loadings for printable composite inks.

1. Introduction

Direct ink writing (DIW) is a rapidly advancing additive manufacturing technology known for its versatility in fabricating complex functional structures with a wide range of materials.[1–3] By utilizing polymer-particle composite inks, DIW has the potential to revolutionize fields such as flexible electronics, biomedical devices, and advanced manufacturing by enabling the creation of structures with tailored mechanical, electrical, and thermal properties.[4–9] The integration of submicron and nanoscale particles into these inks introduces a new realm of functionality, allowing for the fine-tuning of material properties to meet specific application needs.[10–13]

Nanoparticles, due to their high surface area-to-volume ratio and unique properties, have become a focal point in the development of composite inks. These particles are often functionalized to improve compatibility with polymer matrices, enhance dispersion, and achieve specific interactions that can significantly impact the resulting material properties.[14–17] Xu et al. investigated the integration of fumed silica nanoparticles into a silicone rubber matrix reinforced with NdFeB particles to enhance the performance of magnetically active soft materials (MASMs) for DIW applications.[18] The incorporation of these nanoparticles significantly improved the rheological behavior, mechanical strength, and magnetic properties of the MASM inks. Wang et al. utilized silica nanoparticles in their phase-change-enabled DIW ink formulation, where the nanoparticles enhanced the ink's rheological properties by interacting with the wax microparticles.[8] This functionalization allowed for precise control over the ink's flow and solidification, resulting in high-resolution printing with excellent shape fidelity. Kwon et al. developed an innovative approach for manufacturing all-printed nanomembrane hybrid electronics, incorporating functionalized conductive graphene (FCG) as a key material.[19] The FCG was functionalized to enhance biocompatibility, prevent oxidation, and improve solderability, which allowed for the seamless integration of flexible circuits in wearable devices. Hossain et al. explored the incorporation of nano-alumina (NA) into alumina-based inks to enhance solid loading and sinterability in extrusion-based 3D printing.[20] The inclusion of nanoparticles significantly influenced the rheological properties of the inks, where NA contributed to reducing viscosity at lower concentrations through a nano-ball-bearing effect, facilitating better flow during printing. However, at higher concentrations, NA led to increased viscosity due to nanoparticle agglomeration. Therefore, the challenge lies in optimizing the size and loading of these nanoparticles within the ink to ensure not only the desired functionality but also the printability of the ink.

Y. Li, A. Flynn, C. Masternick, B. Kolanovic, B. Li
Department of Mechanical Engineering
Villanova University
Villanova, PA 19085, USA
E-mail: bo.li@villanova.edu
Y. Li, A. Flynn, C. Masternick, B. Kolanovic, B. Li
Hybrid Nano-Architectures and Advanced Manufacturing Laboratory
Villanova University
Villanova, PA 19085, USA
B. Li
Department of Mechanical Engineering
Wichita State University
Wichita, Kansas 67260, USA
E-mail: Bin.Li@wichita.edu

The ORCID identification number(s) for the author(s) of this article can be found under https://doi.org/10.1002/admt.202401443

DOI: 10.1002/admt.202401443

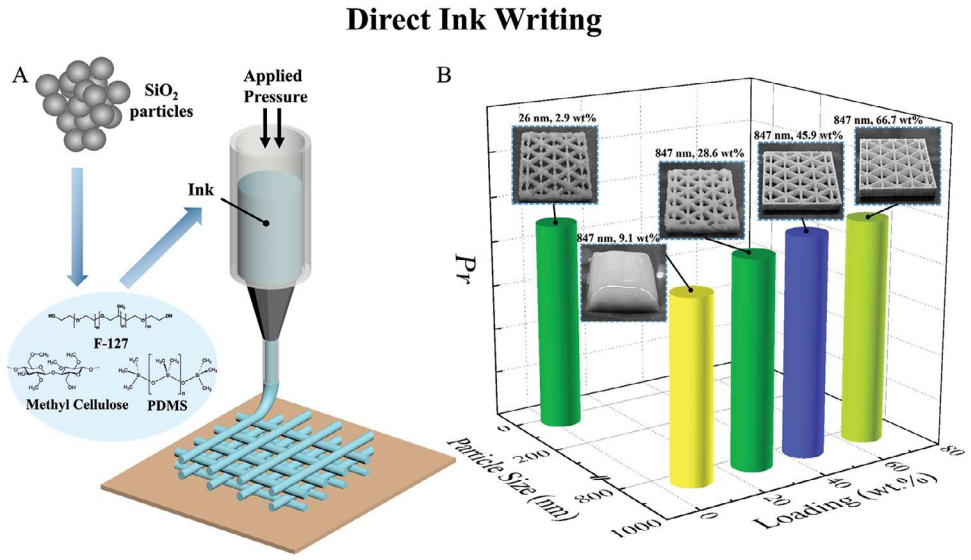

Figure 1. Schematic illustration of DIW process and relationship between SiO_2 loading, size, and printability. A) A simplified diagram illustrating the simple DIW printing technology and experimental design of this work. B) The diagram illustrates the correlation between SiO_2 size and loading in the ink and the structural integrity of the printed objects. Featured images are the cubic structures with dimensions of 15 mm × 15 mm × 5 mm, incorporating a triangular infill pattern with a spacing of 3 mm between each infill. On the image, the text specifies the size and loading of SiO_2 contained in the ink.

Printability, which is defined as the ability of an ink to be extruded and deposited accurately while maintaining the desired shape and structural integrity, is a critical factor in DIW processes.[21,22] Various approaches have been used to assess printability, typically focusing on qualitative measures such as visual inspection of printed lines and structures, and ink rheology. Andrew et al. investigated the extensional and shear rheology of graphene oxide (G.O.) suspensions, focusing on three key rheological parameters: storage modulus, solid-liquid transition stress, and the flow transition index.[23] These parameters were utilized to predict the printability of the G.O. suspensions, offering insights into how the material behaves during the printing process, particularly in terms of extrusion and shape retention. Ji et al. developed a novel experimental approach to evaluate the printability of inks prepared from water-based slurries of Al_2O_3, Y_2O_3, and Nd_2O_3 ceramic powders.[24] They utilized rotational and capillary rheology tests, focusing on parameters such as storage modulus and extrusion stress, to assess ink quality for direct ink writing. Their findings quantitatively defined optimal printability ranges and provided insights into bubble suppression during extrusion. Chen et al. employed machine learning (ML) algorithms, including decision tree, random forest (RF), and deep learning (DL), to predict the printability of biomaterials, addressing the complexities and inefficiencies associated with the traditional trial-and-error approach in developing 3D-printable inks.[25] Such methods are crucial for optimizing ink formulations, particularly when working with a wide range of nanoparticle sizes and loadings. Despite the importance of these factors, there is a lack of comprehensive studies that systematically evaluate how variations in nanoparticle size and loading impact the printability of composite inks in DIW processes.

To address these gaps, our work systematically investigates the effects of SiO_2 nanoparticle size, ranging from as small as 26 nm to as large as 847 nm, and particle loading (1.0–66.7 wt.%) in a polydimethylsiloxane (PDMS) matrix. We aim to understand how these variables influence the overall performance of the composite inks, with a particular focus on their printability. To examine the printability in different printing structures, we employ three complementary methods: 3D printing line analysis (3D-PLA), dual-layer printing analysis (DLPA), and ink rheology analysis (IRA). These methods provide a comprehensive assessment of how nanoparticle size and loading affect the ink's ability to be extruded, and its shape retention postprinting. By exploring these aspects, we aim to define a design space for DIW that optimizes the printability of polymer-particle composite inks. Our findings provide valuable insights into how nanoparticle size and loading affect printability, offering guidelines for optimizing ink formulations to achieve the desired printability. This work enhances the understanding of DIW technology's capabilities in producing high-quality prints, thereby broadening its potential applications in advanced manufacturing.

2. Results and Discussion

2.1. DIW Printing of Composite Ink Containing SiO_2 Nanoparticles

In **Figure 1A**, the DIW process of composite ink containing SiO_2 particles (ranging from nanosize to submicron) and PDMS is illustrated. To demonstrate the effect of particle size on printability, two SiO_2 particle sizes (26 and 847 nm in diameter) were selected to print several samples for comparison. For 847 nm particles, a clear trend of increased printability can be observed in Figure 1B with increasing particle loading under a constant printing pressure of 50 psi (3.4×10^6 Pa). At a loading of 9.1 wt.%, the printed lines merged, indicating poor printability. A loading of 28.6 wt.% resulted in a sample with decent shape stability, indicating moderate printability, while the maximum extrudable loading under

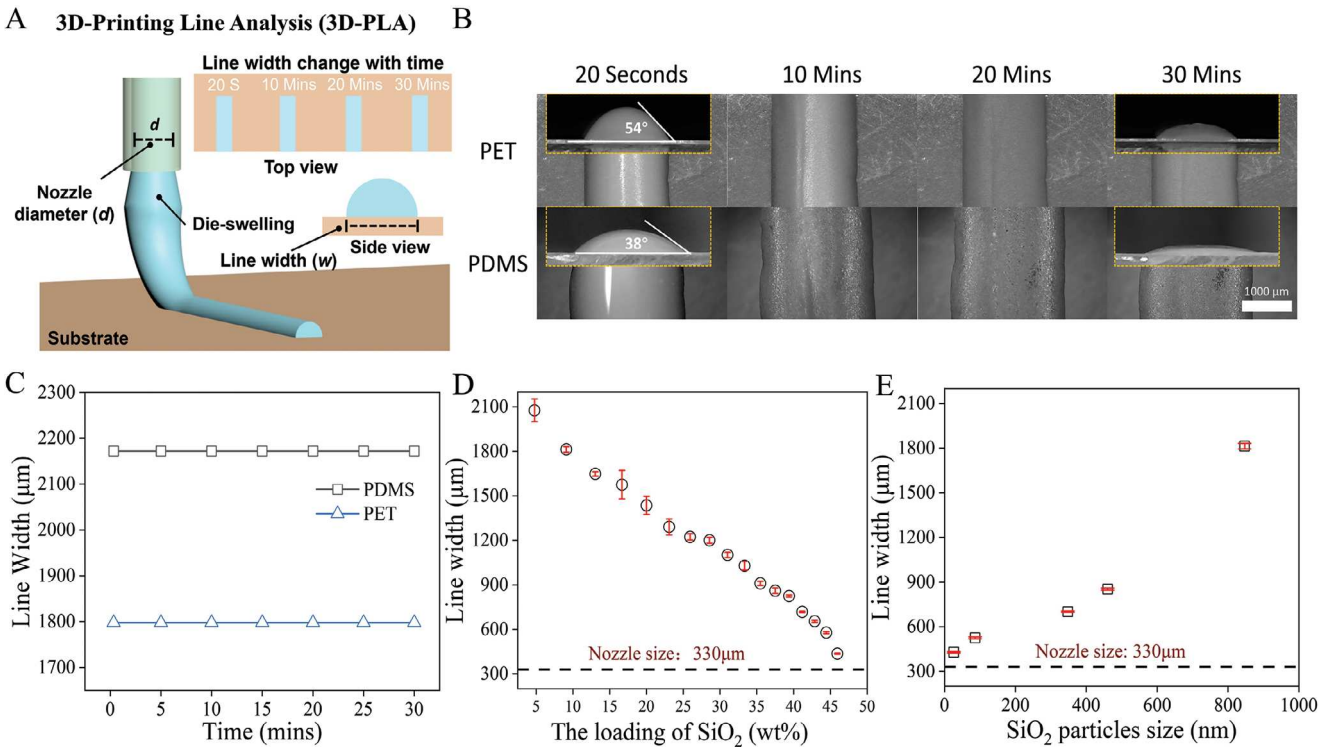

Figure 2. 3D-PLA for the printability evaluation of the first layer. A) A simplified diagram illustrating the 3D-PLA method. B) Comparative analysis of line width variation over 30 min on Polyethylene terephthalate (PET) and PDMS substrates. Embedded images show side views of the printed lines at 20 s and 30 min postprinting, scale bar represents 1000 μm. C) Graphical representation of the stability of line widths across different substrates over a 30-min period. D) Correlation between line width and SiO_2 particle loading, ranging from 4.8 to 45.9 wt.%. The size of the particles was 847 nm. E) Correlation between line width and SiO_2 particle sizes (26, 86, 348, 460, 847 nm). The loading of the inks was 9.1 wt.%.

50 psi was 45.9 wt.%, which showed even better printability. Further increasing the pressure to 120 psi (8.3×10^6 Pa) allowed for a higher loading of 66.7 wt.%, resulting in the best printability observed. When the particle size was reduced to 26 nm, good printability was achieved with a minimum loading of only 2.9 wt.%. In contrast, achieving a similar appearance with 847 nm particles required a loading of 28.6 wt.% or higher. This demonstrates the tunability of particle size and loading in optimizing printability. However, it should be noted that visual evaluation alone cannot provide a quantitative measure of printability highlighting the need for a systematic and quantitative study of the printability of nanoparticle-filled composite inks.

2.2. 3D-PLA for the Printability Evaluation of the One-Layer Printing

In DIW printing, the first printed layer is essential and in many applications, only one layer is needed. For example, conductive inks can be printed into thin electrodes.[17,26] In multilayer printing, a stable interface between the first layer and the substrate is the foundation for stacking succeeding layers. For example, if such an interface is weak, the shrinkage of the printed part caused by solvent evaporation can detach the part from the substrate.[27] To assess the printability of one-layer printing, printed line width analysis (PLWA) has been widely utilized. For instance, Giuseppe et al. demonstrated that higher concentrations of alginate-gelatin blends lead to narrower strand widths due to increased viscosity, directly impacting the accuracy of the print.[28] Similarly, Göhl et al. employed simulations to predict the impact of varying printing parameters on line resolution, a key factor in determining the mechanical properties of printed structures.[29] Additionally, Lee et al. found that different types of gelatin methacrylate (GelMA) exhibited varying line widths under the same conditions, highlighting the sensitivity of printability to material properties.[30] These studies underscore the critical role of PLWA in ensuring the precision and stability of the printed layers. However, the time-dependent wetting and evaporation process may affect the printed lines which were not monitored in the current PLWA method.

In this research, we developed a 3D-PLA system as shown in **Figure 2A** to monitor both top and side views of the printed lines with respect to their resting time (t), defined as the time after the landing of lines on the substrate. To evaluate the line resolution aspect of the printability, it is interesting to introduce a parameter of nozzle diameter (d) to the line width (w) ratio. In the polymer extrusion, the extrudate will be larger than the size of the die (nozzle in DIW). This is called die-swell behavior and can be attributed to the viscoelastic behavior of polymers or polymer-containing inks.[31,32] The die swell can be problematic for DIW as a narrow line width or large d/w suggests better resolution. Die swell can be reduced by stretching the extrudate. In the case of DIW, modulating the printing pressure and speed or engineering the composite of the polymer ink can effectively tailor the d/w. In

this study, we focused on the influence of polymer ink (e.g., particle size and loading) with fixed nozzle size ($d = 330$ µm), printing pressure ($P = 50$ psi), and nozzle moving speed ($v = 6$ mm $^{-1}$s).

As shown in Figure 2B,C, we have compared the change of printed line on PET and PDMS substrates along with the resting time (t). Here, the polymer ink containing 9.1 wt.% 847 nm SiO_2 particles was chosen. The printed pattern consisted of five parallel 3-cm-long lines. At $t = 20$ s, the line width on PDMS is 2172 µm, while that on PET is 1810 µm. The contact angles from the side view images show a better affinity of ink with PDMS substrate (38°) than PET substrate (54°) (Figure 2B). Such difference can be explained by the better wetting capability of PDMS-based ink on a PDMS substrate. Intuitively, the ink with low viscosity may spread over the substrate after printing leading to poor printability. But it is surprising to note that the first side view images for both substrates were taken at $t = 20$ s and the width has not changed ever since (Figure 2C). The results suggest the wetting happens immediately after the lines touch the substrates and quickly reaches an equilibrium. The wetting between the line and substrate critically determines the line resolution.[33] The side view images in Figure 2B suggest that the evaporation of solvent will only reduce the height of the line, while the edges of the lines do not retract during evaluation. This phenomenon suggests strong confinement from the substrate for one-layer printing.

As shown in Figure 2D, the influence of particle loading was studied by expanding the loading of 847 nm SiO_2 particles from 4.8 to 45.9 wt%. On PET substrate, the line width reduced from 2068 µm ($d/w = 0.16$) to 436 µm ($d/w = 0.76$). If loading of SiO_2 particles is fixed at 9.1 wt.%, by reducing the particle size from 847 to 26 nm, a significant reduction of the line width from 1810 µm ($d/w = 0.18$) to 429 µm ($d/w = 0.77$) was achieved (Figure 2E). This trend suggests that increased particle loading and reduced particle size can reduce the line width leading to better printing resolution. The fundamental physics can be further elaborated using the IRA measurement in Section 2.4.

The 3D-PLA method which captures the 3D time-of-flight interaction of ink and substrates represents an important innovation in evaluating the ink printability and line resolution in the one-layer printing process. It includes big metrics of parameters from material design, choice of substrate, and printing processes. However, when the printing reaches the second layer, the "supporting substrate" of the second layer changes from a homogenous surface to the printed first layer which is a hybrid structure of polymer gel and air gaps. Additionally, the merging between layers will complicate the situation which limits the capability of the 3D-PLA method in evaluating the printability of ink in 3D structures.

2.3. Evaluation of DLPA for Multilayer Printing

As the DIW process advances with the stacked layers, the interactions between these successive ink layers gain paramount importance, significantly impacting the overall structural integrity and quality of the printed output. DLPA utilizes a two-layer platform to quantify printability (Pr) considering inter-layer interactions as shown in **Figure 3A**. Dual-layer constructs were printed with the same distance between adjacent filaments both in the x- and y-directions. We first define the circularity (C) using following Equation (1):

$$C = \frac{4\pi A}{L^2} \tag{1}$$

where L and A are the perimeter and area of the pores, respectively. The Pr of ink based on a printed square shape is defined using Equation (2):

$$Pr = \frac{\pi}{4}\frac{1}{C} = \frac{L^2}{16A} \tag{2}$$

In an ideal case, the shape of the extruded filament will remain stable even if another layer of filament is deposited on top of it, resulting in the formation of square holes and $Pr = 1$. In reality, driven by the gravitational force and tendency to reduce the surface energy, the two layers of the filament will fuse leading to $Pr < 1$, and according to current research on DIW printability, $Pr = 0.9$ is set as an empirical threshold beyond which the 3D printed construct is considered as mechanically stable.[34,35]

A systematic study was performed using submicron and nanoparticles with different sizes (from 26 to 847 nm) and loadings. The printing parameters were fixed unless stated otherwise: pressure = 50 psi, nozzle moving speed = 6 mm s^{-1}, nozzle size = 330 µm, and substrate was PET. Figure 3B shows representative optical images of printed dual layer construct with the same particle loading (9.1 wt.%) but different sizes (26–847 nm). Clearly, Pr increases with the decreased particle size. The data for the smallest (26 nm) and the largest (847 nm) particles are shown in Figure 3C,D, respectively. Consistently, higher loading leads to larger Pr values for all particles. It is important to note that the smallest nanoparticles (26 nm) pass the threshold ($Pr = 0.9$, dash line) with a minimal loading of 2.9 wt.%, which is ≈10 times smaller compared to a minimal loading of 28.6 wt.% for the 847 nm particles. Such contrast can be attributed to the significantly increased surface-to-volume ratio of smaller particles.[36,37] Figure 3E further compares Pr for multiple particles at fixed loadings. Such comparison confirms consistent trends where Pr increases with decreased particle size and increased loadings.

Unlike 3D-PLA which is strongly influenced by the substrate, DLPA emphasizes the inter-layer interaction. However, the first layer of the DLPA construct is in direct contact with the substrate, and its cross-section and line width are affected by the substrate. Therefore, it is important to investigate the substrate dependency of DLPA. As shown in Figure 3C (red stars), for 847 nm particle system, three representative loadings (i.e., 9.1 wt.%, the lower bound; 28.6 wt.%, the first loading value exceeding $Pr = 0.9$; and 45.9 wt.%, the maximum loading at 50 psi) were picked to repeat the DLPA measurement on PDMS substrates. The overlapping Pr for different loadings reveals that the choice of substrate, whether PET or PDMS, has minimal influence on the DLPA results. Such comparison suggests DLPA mainly reflects the inter-layer interaction of the printed lines and can be a generic method to quantitatively compare the printability of different ink formulas. Although the choice of the threshold value ($Pr = 0.9$) of DLPA is empirical, the ink formula with similar Pr (e.g., $Pr_{26\text{ nm-}2.9\text{ wt\%}} = 0.91$ vs $Pr_{847\text{ nm-}28.6\text{ wt\%}} = 0.91$) does show similar sample

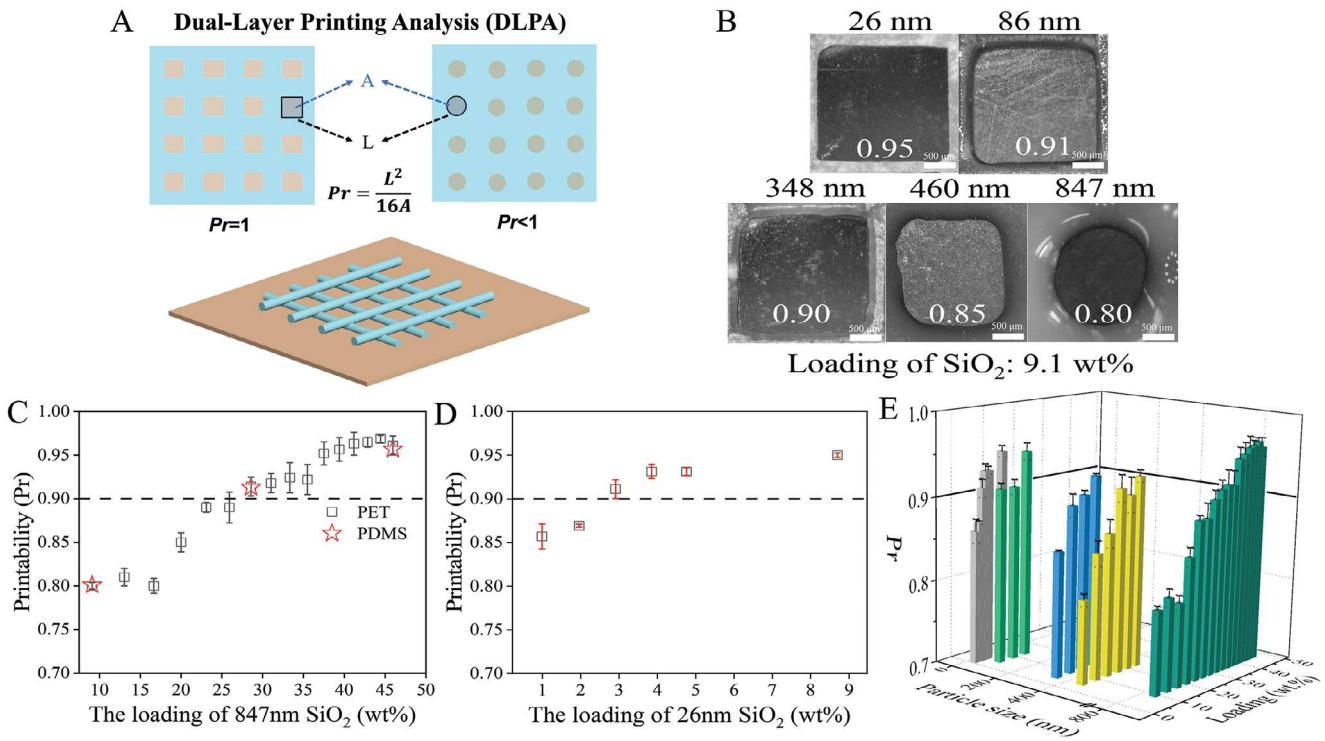

Figure 3. Evaluation of DLPA. A) A simplified diagram illustrating the DLPA method and the cases where printability is less than 1 and equal to 1. B) Enlarged images of dual-layer structures after printing, displaying different particle sizes (26, 86, 348, 460, 847 nm) with the same loading (9.1 wt.%). The white color numbers in the images correspond to the *Pr* values, scale bar represents 500 µm. C) Relationship between loading and *Pr* for ink containing 847 nm SiO_2 particles, with $Pr \approx 0.9$. D) Relationship between loading and *Pr* for ink containing 26 nm SiO_2 particles, with $Pr \approx 0.9$. E) Impact of five different sizes of SiO_2 particles on ink *Pr* value at varying loadings.

appearances as shown in Figure 1B. In addition, such threshold value has root from the rheological behavior of the ink as demonstrated in the following section.

2.4. Evaluation of IRA

The printing process and ink printability are directly related to the rheological properties of inks. Understanding the relationship between desirable rheological characteristics and subsequent satisfactory printability is critical.[38–40] For example, M'Barki et al. developed a dimensionless criterion to predict printability in dense ceramic objects by monitoring the evolution of rheological properties over time, allowing for the rational design of inks based on deformation predictions.[39] Similarly, Gao et al. investigated the printability of gelatin-alginate hydrogels, demonstrating that the balance between storage modulus (G′), loss modulus (G″), and their ratio (tanδ) critically affects extrudability and structural integrity.[41] Additionally, Lewis et al. emphasized the importance of tailoring ink rheology to achieve specific behaviors during droplet and filament-based DIW, highlighting the need for inks to maintain suitable rheological properties throughout the printing process to ensure high-quality assembly.[42] Here, IRA was conducted near the empirical DLPA printability threshold ($Pr = 0.9$) in the hope of acquiring the key rheological characteristics demanded by DLPA printability, and their relations with 3D-PLA.

Die swell and the effects of gravity on the resting inks are crucial to line resolution, shape retention, and self-supporting capacity of the extruded filaments. Die swelling is associated with polymer chain relaxation, and it commonly exists in polymer extrusion and DIW of polymeric inks. The presence of solid particles can suppress the motion and relaxation of polymer chain networks and reduce die swell, improving line resolution.[43] Such chain network retardancy will be further enhanced by the geometric confinement of the particle network, with increasing particle loading and reducing particle size to the nanoscale.[44] Both factors, at the same time, also endow the inks with more solid-like behaviors with good shape retention and resistance to gravity.

Typically, a solid-like behavior is indicated by a dominating elastic character, or a tan ($\boldsymbol{\delta}$) ($= G''/G'$) lower than 1, where G' is the storage modulus, equivalent to the elastic modulus of a solid material, G'' is the loss modulus, quantifying the liquid-like viscous character of a viscoelastic material. Their ratio, i.e., tan ($\boldsymbol{\delta}$), is frequently used to study the gelation process in gels and nanocomposites.[40] With a gelation point defined by tan ($\boldsymbol{\delta}$) = 1, tan ($\boldsymbol{\delta}$) < 1 suggests the presence of continuous network structures and resulting solid-like elastic dominant behaviors.

Viscoelastic properties of the inks by oscillation amplitude sweep tests are presented in **Figure 4** and **Table 1**. The linear viscoelastic region (LVR) can be used to simulate the resting state of the extruded inks.[38,40] The nanocomposite ink

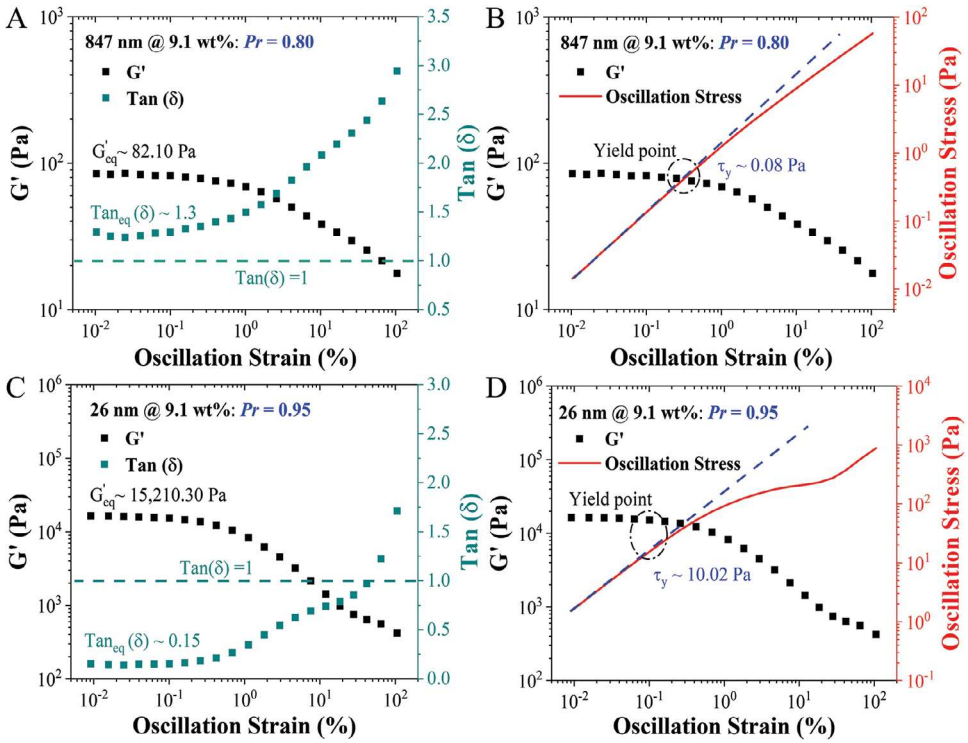

Figure 4. Rheological properties of selected composite inks. A,B) Composite ink with *Pr* lower than 0.9. C,D) Composite ink with *Pr* higher than 0.90.

containing 9.1 wt.% 847 nm particle (Figure 4A) exhibited a high tan (**δ**) value of 1.30 in LVR region (denoted as tan $(\boldsymbol{\delta})_{eq}$), in contrast to the ink containing 9.1 wt.% 26 nm particle with a tan $(\boldsymbol{\delta})_{eq}$ of 0.15 (Figure 4C). Such a drastic difference is attributed to the stronger networking capability of smaller particle, because of a larger number of particles and higher surface areas,[45] which also accounts for the much higher G′ in LVR (denoted as G'_{eq}), that is, ≈15 200 Pa for the ink with 26 nm particle versus ≈82 Pa for the ink with 847 nm particles, at the same 9.1 wt.% loading. Additionally, yield stress ($\boldsymbol{\tau}_y$), that is, the stress at the limit of LVR region indicating the breakdown of internal structures and resulting permanent deformation, was significantly elevated to ≈10.02 Pa (Figure 4D) from ≈0.15 Pa (Figure 4B). However, it should be noted that there are two breakdown mechanisms responsible for the end of the LVR region. In the ink with 9.1 wt.% 847 nm SiO_2 particles, it is related to the disentanglement of the polymer chains; while in the ink with 9.1 wt.% 26 nm SiO_2 particles, the breakdown of SiO_2 network dominates this transition.

Obviously, the continuous SiO_2 network contributes to a more solid and stronger ink, and eventually, better ink printability and line resolutions as revealed in Sections 2.2 and 2.3. Besides reducing particle size, increasing the particle loading also favors the formation of SiO_2 network. As shown in Table 1, a similar trend of key rheological parameters is also observed with loading much more 847 nm particles. However, due to the stronger network capability of 26 nm SiO_2 nanoparticles, to achieve similarly high line resolution, as shown in Figure 2, and good ink printability, as shown in Figure 3, much lower nanoparticle loading is needed. Such dependencies of ink printability and resolution on the size and loading of nanoparticles are further supported by the rheological properties of the inks loaded with 460 nm SiO_2 as in Table 1. The amount of 460 nm nanoparticle needed for an effectual SiO_2 network is ≈16.7 wt.%, in between those for 26 and 847 nm nanoparticles.

By correlating the key rheological parameters and DLPA printability in Table 1, it is found that a tan $(\boldsymbol{\delta})_{eq}$ value of ≈0.4 or lower appears to be associated with a printability higher than 0.9. In the meantime, to counter the effects of gravity on shape retention, minimum G'_{eq} and $\boldsymbol{\tau}_y$ are expected to be close to ≈1000 Pa and 2 Pa, respectively. Higher G'_{eq} and $\boldsymbol{\tau}_y$, with increasing loading of SiO_2 particles, indicates that gravity has weak influences on the ink at rest, and can be related to the better printability of the ink and line resolution.

Table 1. Summary of key rheological parameters of inks ≈0.9 *Pr* threshold.

	Loading	Tan_{eq} [**δ**]	G'_{eq} [Pa]	$\boldsymbol{\tau}_y$ [Pa]	*Pr*
26 nm	1.0 wt.%	1.42	54.20	0.15	0.86
	2.9 wt.%	0.38	1540.40	2.58	0.91
	9.1 wt.%	0.15	15 210.30	10.02	0.95
460 nm	4.8 wt.%	1.08	35.53	0.83	0.80
	16.7 wt.%	0.45	930.24	2.47	0.91
	23.1 wt.%	0.34	3696.58	6.07	0.93
847 nm	9.1 wt.%	1.30	82.10	0.08	0.80
	25.9 wt.%	0.41	4719.80	5.12	0.89
	31.0 wt.%	0.25	18 900.30	30.80	0.92
	66.7 wt.%	0.10	36 172.10	71.40	0.98

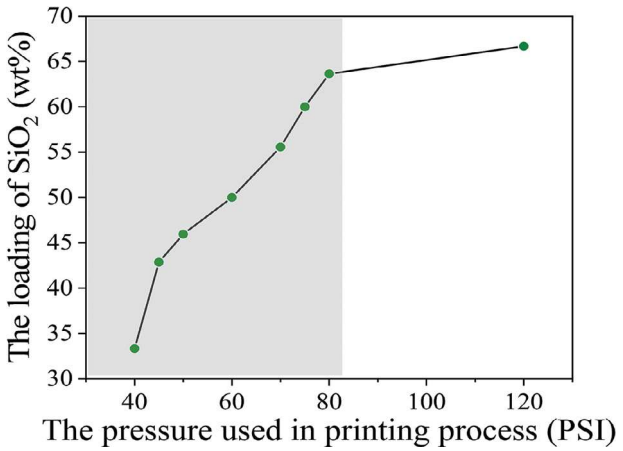

Figure 5. The relationship between different pressure values and the maximum achievable loading for successful printing using ink formulations containing 847 nm SiO_2 particles under the conditions of a 330 μm nozzle size and a printing speed of 6 mm s^{-1}. The surface morphology and Raman spectrum information of the sample printed with ink containing 847 nm SiO_2 at maximum loading (66.7 wt.%) are presented in support information (Figure S3, supporting information).

2.5. Explore the Design Space of Composite Ink

This intriguing observation in *Pr*'s size and loading dependency highlights the capability of tailoring the properties of 3D printed structures. Reducing particle loading can save expensive nanomaterials and is desired for many applications requiring the gel-like behavior of the part. In this study, under an extrusion pressure of 50 psi, the minimum loading to pass the threshold ($Pr = 0.9$) is achieved using 26 nm particles at 2.9 wt%. On the other hand, pushing the system to the maximum loading leads to better shape stability, narrower line width, and higher printing resolution. More importantly, with the increased ceramic components, the mechanical properties can be enhanced and open the gate toward "rigid" applications such as artificial bones. Based on the discussion before, the maximum printable loading would be achieved with 847 nm particles.

Here, we redefine the standard to judge the maximum printable loading. The theoretical upper limit of particle loading in an extrusion process can be defined as the point beyond which the viscosity of the ink is too high to be extruded out. However, in reality, increased loading will cause instability of extrusion forming discontinuous lines or rough surfaces before reaching the theoretical limit. Therefore, we define the maximum loading as the point before the transition from a continuous smooth line to a discontinuous/rough line to judge the upper limit. The experimental details can be found in the supporting information (Tables S1 and S3, supporting information).

As shown in **Figure 5**, the maximum loading of the ink increased from 33.3 wt.% at 40 psi to 66.7 wt.% at 120 psi. More importantly, the steep slope in the range of 40–80 psi suggests pressure modulation is effective in increasing the maximum loadings. However, the reduced slope between 100 and 120 psi suggests that as the loading increases, the effectiveness of pressure modulation reduces. Unfortunately, 120 psi was the upper limit of the commercial 3D printer used in this study. However, our result suggests that the pressure modulation may eventually reach a plateau where particle loading cannot be further increased. It is interesting to note that as water is used as the solvent, the maximum loading of 847 nm particles can further increase to 82.1 wt.% after drying the water.

3. Conclusion

This study aimed to evaluate the printability of inks containing different sizes and loadings of SiO_2 micro- and nanoparticles according to different printing structures: monolayer printing versus 3D printing. Both 3D-PLA and DLPA suggest smaller particles and larger loading help increase printability. 3D-PLA is suitable for evaluating the printability of monolayer structures and the influence of supporting substrates. DLPA focused on the merging of the stacking layers and was independent of the choice of substrate. IRA reveals the fundamental physics of network formation of nanoparticles and helps correlate the rheological behavior of composite ink with printability in 3D-PLA and DLPA. Considering $Pr = 0.9$ as a threshold and at 50 psi, a minimum loading of 2.9 wt.% for 26 nm particles is required, while to achieve a similar *Pr*, 28.6 wt.% is needed for 847 nm particles. We have also explored the higher bound of the loading and found the maximum loading is 66.7 wt.% at a maximum pressure of 120 psi. Increasing the pressure may further increase the maximum loading but there might be a plateau.

In summary, our study contributes to the advancement of additive manufacturing by providing insights into ink formulation and parameter optimization for achieving high printability. The findings underscore the potential of nanoparticles in tailoring ink properties and emphasize the importance of establishing standardized evaluation criteria for reliable and efficient 3D printing processes. Future research efforts can focus on exploring additional parameters and particle characteristics to further enhance printability and expand the application possibilities of DIW materials.

4. Experimental Section

Materials: The materials used in the experiments were as follows: Pluronic F-127 (Sigma-Aldrich, USA), Methyl cellulose (viscosity 1600 cPs, Beantown Chemical Company, USA), Polydimethylsiloxane (PDMS) (Sylgard 184, Dow Corning, USA), Spherical SiO_2 particles (vendor-labeled 20, 60, 200, 400, and 800 nm, US Research Nanomaterials Inc., USA).

Preparation of Polymer-Particle Composite Inks—Pluronic F-127 Solution Preparation: Pluronic F-127 was mixed with deionized (DI) water at a 40:100 weight ratio. The mixture was stirred using a magnetic stirrer (Stirrer 365, VWR, USA) for 30 minutes, then, the mixture was transferred to a refrigerator at 4 °C overnight, resulting in a clear and transparent solution.

Preparation of Polymer-Particle Composite Inks—Methyl Cellulose (MC) Gel Preparation: MC was mixed with deionized water (2:100 in weight). The mixture was stirred using a magnetic stirrer (Stirrer 365, VWR, USA) for 2 h. After stirring, the mixture settled at room temperature for 24 h, yielding a clear and homogeneous MC gel.

Preparation of Polymer-Particle Composite Inks—PDMS Preparation: PDMS was prepared by mixing Sylgard 184 base and curing agent (10:1 in weight). The mixture was thoroughly stirred and then placed in a vacuum chamber for bubble removal under vacuum conditions.

Preparation of Polymer-Particle Composite Inks—Composite Ink Preparation: The synthesized F-127 solution, MC gel, and PDMS were mixed at a weight ratio of 1:1:1. This mixture leverages the surfactant and rheology

modifying properties of F-127 to stabilize the ink mixture and improve its flow characteristics.[46,47] MC gel contributes to the ink's thermal gelling behavior, enhancing printability by providing controlled viscosity and water retention.[48,49] PDMS adds flexibility and mechanical integrity to the printed structures, as well as making them more durable.[50–52] The mixture was thoroughly stirred and used as a polymer base for the composite ink. The weight of the polymer base was fixed at 100 g and a predetermined amount of SiO_2 submicron and nanoparticles was added to the polymer base. For example, if 3 g of SiO_2 was added, the particle loading is 2.9 wt.%. The detailed calculations of the loading for different formulas were summarized in Table S1 (Supporting Information). After uniform mixing, the ink was transferred to a 5 mL syringe (Allevi Inc., USA). The syringe containing the ink was subjected to centrifugation at a speed of 3000 revolutions per minute (rpm) for 30 min to remove any air bubbles. After centrifugation, the ink was stored in a refrigerator at 4 °C overnight before being printed.

Printing of Polymer-Particle Composite Inks: A luer-lock plastic blunt-end tip (330 µm) was attached to the syringe and then loaded into the printing head. The ink was printed using direct ink writing 3D printer (Allevi 3 Bioprinter, Allevi Inc., USA). A compressed air pneumatic system was used to pressurize the syringe barrel and control the ink flow rate. Unless noted otherwise, the printing parameters were fixed: 6 mm s^{-1} for printing speed (i.e., nozzle moving speed), 50 psi (3.45×10^5 Pa) for pressure, 23 °C for printing temperature, and PET film as the substrate and 330 µm for nozzle diameter (*d*).

Characterizations: The sizes of the SiO_2 submicron and nanoparticles used in the study were characterized using dynamic light scattering at 25 °C with a particle size analyzer (NanoBrook Omni, Brookhaven Instruments, USA) (Figure S1 and Table S2, supporting information). The optical images of line width and cross section for 3D-PLA and merged dual-layer construct in DLPA were obtained immediately after printing using an optical microscope (TM-DM11, Tomlov, USA). The samples were not cured before imaging to capture the initial printed structure's morphology. Following the imaging, the samples were further cured by being left at room temperature for 48 h to ensure the stability of the printed structures. Image analysis was conducted using ImageJ software (version: ImageJ 1.53K). The printed structures were characterized using Hitachi S-4800 scanning electron microscope (SEM). The accelerating voltage was 20 kV, and the working distance was 18.6 mm (Figure S3, supporting information). Raman spectroscopy was conducted using a confocal Raman microscope (Alpha 300R, Witec, Germany) with 532 nm laser, 10× objective, and 1200 g mm^{-1} grating. The spectrum was acquired over 5 s per accumulation at 10% laser power and averaged over 5 accumulations (Figure S3, supporting information). Discovery HR-2 rheometer, TA, was used for rheological analysis of the composite ink through oscillation mode. The storage modulus (G′) and loss moduli (G″) were obtained via oscillation amplitude sweeps at a frequency of 10 rad s^{-1} at 25 °C over a range of oscillation strain from 0.01% up to 100%.

Supporting Information

Supporting Information is available from the Wiley Online Library or from the author.

Acknowledgements

This work was supported by the National Science Foundation (Grant No. 2221102, No. 2018852), Villanova University Startup Fund, and the University Summer Grant of Villanova University. A.F., C.M., and B.K. were supported by the Small Research Pilot Grant and Small Research Grant of Villanova University.

Conflict of Interest

The authors declare no conflict of interest.

Author Contributions

Y.L. performed conceptualization, data curation, formal analysis, investigation, methodology, project administration, supervision, validation, and visualization, wrote the original draft, and wrote, reviewed, and edited. A.F. performed data curation, formal analysis, and investigation, and wrote the original draft. C.M. performed Data curation and investigation and wrote the original draft. B.K. performed data curation, and investigation, and wrote the original draft. B.L. performed conceptualization, data curation, formal analysis, visualization, Writing-original draft, wrote, reviewed, and edited, Resources. B.L. performed conceptualization, data curation, formal analysis, visualization, supervision, project administration, and resources, wrote the original draft, wrote, reviewed, and edited, and funding acquisition.

Data Availability Statement

The data that support the findings of this study are available from the corresponding author upon reasonable request.

Keywords

direct ink writing, ink rheology, polymer-particle composite inks, printability

Received: August 31, 2024
Revised: December 13, 2024
Published online:

[1] R. L. Truby, J. A. Lewis, *Nature* **2016**, *540*, 371.
[2] X. Peng, X. Kuang, D. J. Roach, Y. Wang, C. M. Hamel, C. Lu, H. J. Qi, *Addit. Manuf.* **2021**, *40*, 101911.
[3] E. Din, *ISO/ASTM 52900: 2021 Additive Manufacturing—General Principles—Fundamentals and Vocabulary*, Beuth Verlag GmbH, Berlin **2021**.
[4] J. A. Lewis, *Adv. Funct. Mater.* **2006**, *16*, 2193.
[5] V. G. Rocha, E. Saiz, I. S. Tirichenko, *J. Mater. Chem. A* **2020**, *8*, 15646.
[6] X. Wan, L. Luo, Y. Liu, J. Leng, *Adv. Sci.* **2020**, *7*, 2001000.
[7] Z. Jiang, O. Erol, D. Chatterjee, W. Xu, N. Hibino, L. H. Romer, S. H. Kang, D. H. Gracias, *ACS Appl. Mater. Interfaces* **2019**, *11*, 28289.
[8] Y. Wang, N. Willenbacher, *Adv. Mater.* **2022**, *34*, 2109240.
[9] T. N. H. Nguyen, J. K. Nolan, H. Park, S. Lam, M. Fattah, J. C. Page, H.-E. Joe, M. B. G. Jun, H. Lee, S. J. Kim, R. Shi, H. Lee, *Biosens. Bioelectron.* **2019**, *131*, 257.
[10] A. C. H. Tsang, J. Zhang, K. N. Hui, K. S. Hui, H. Huang, *Adv. Mater. Technol.* **2022**, *7*, 2101358.
[11] D. Behera, M. Cullinan, *Prec. Engin.* **2021**, *68*, 326.
[12] D. Ravichandran, W. Xu, M. Kakarla, S. Jambhulkar, Y. Zhu, K. Song, *Addit. Manuf.* **2021**, *47*, 102322.
[13] D. Lei, Y. Yang, Z. Liu, S. Chen, B. Song, A. Shen, B. Yang, S. Li, Z. Yuan, Q. Qi, L. Sun, Y. Guo, H. Zuo, S. Huang, Q. Yang, X. Mo, C. He, B. Zhu, E. M. Jeffries, F.-L. Qing, X. Ye, Q. Zhao, Z. You, *Mater. Horiz.* **2019**, *6*, 394.
[14] S. Saska, L. Pilatti, A. Blay, J. A. Shibli, *Polymers* **2021**, *13*, 563.
[15] Q. Chen, P. F. Cao, R. C. Advincula, *Adv. Funct. Mater.* **2018**, *28*, 1800631.
[16] L.-Y. Zhou, Q. Gao, J. Fu, Q. Chen, J. Zhu, Y. Sun, Y. He, *ACS Appl. Mater. Interfaces* **2019**, *11*, 23573.
[17] Q. Shi, H. Chen, K. Pang, Y. Yao, G. Su, F. Liang, N. Zhou, *J. Mater. Chem. C* **2020**, *8*, 15099.
[18] Z. Xu, X. Wang, F. Chen, K. Chen, *ACS Appl. Polym. Mater* **2023**, *5*, 5794.

[19] Y.-T. Kwon, Y.-S. Kim, S. Kwon, M. Mahmood, H.-R. Lim, S.-W. Park, S.-O. Kang, J. J. Choi, R. Herbert, Y. C. Jang, Y.-H. Choa, W.-H. Yeo, *Nat. Commun.* **2020**, *11*, 3450.
[20] S. S. Hossain, B. Gao, S. Park, C.-J. Bae, *ACS Appl. Nano Mater.* **2022**, *5*, 17828.
[21] M. A. S. R. Saadi, A. Maguire, N. T. Pottackal, Md. S. H. Thakur, M. Md. Ikram, A. J. Hart, P. M. Ajayan, M. M. Rahman, *Adv. Mater.* **2022**, *34*, 2108855.
[22] L. Y. Zhou, J. Fu, Y. He, *Adv. Funct. Mater.* **2020**, *30*, 2000187.
[23] A. Corker, H. C.-H. Ng, R. J. Poole, E. García-Tuñón, *Soft Matter* **2019**, *15*, 1444.
[24] H. Ji, J. Zhao, J. Chen, S. Shimai, J. Zhang, Yu Liu, D. Liu, S. Wang, *Addit. Manuf.* **2022**, *55*, 102846.
[25] H. Chen, Y. Liu, S. Balabani, R. Hirayama, J. Huang, *Research* **2023**, *6*, 0197.
[26] M. Abshirini, M. Charara, Y. Liu, M. Saha, M. C. Altan, *Adv. Eng. Mater.* **2018**, *20*, 1800425.
[27] E. A. Slejko, S. Seriani, V. Lughi, *J. Mater. Res.* **2022**, *37*, 773.
[28] M. Di Giuseppe, N. Law, B. Webb, R. A. Macrae, L. J. Liew, T. B. Sercombe, R. J. Dilley, B. J. Doyle, *J. Mech. Behav. Biomed. Mater.* **2018**, *79*, 150.
[29] J. Göhl, K. Markstedt, A. Mark, K. Håkansson, P. Gatenholm, F. Edelvik, *Biofabrication* **2018**, *10*, 034105.
[30] B. H. Lee, N. Lum, L. Y. Seow, P. Q. Lim, L. P. Tan, *Materials* **2016**, *9*, 797.
[31] M. E. Mackay, *J. Rheol.* **2018**, *62*, 1549.
[32] A. Das, E. L. Gilmer, S. Biria, M. J. Bortner, *ACS Appl. Polym. Mater* **2021**, *3*, 1218.
[33] D. A. Rau, M. J. Bortner, C. B. Williams, *Addit. Manuf.* **2023**, *75*, 103745.
[34] L. Ouyang, R. Yao, Y. Zhao, W. Sun, *Biofabrication* **2016**, *8*, 035020.
[35] V. Ozbolat, M. Dey, B. Ayan, A. Povilianskas, M. C. Demirel, *ACS Biomater. Sci. Eng.* **2018**, *4*, 682.
[36] I. Khan, K. Saeed, I. Khan, *Arabian J. Chem.* **2019**, *12*, 908.
[37] L. Nayak, S. Mohanty, S. K. Nayak, *J. Mater. Chem. C* **2019**, *7*, 8771.
[38] A. Schwab, R. Levato, M. D'Este, S. Piluso, D. Eglin, J. Malda, *Chem. Rev.* **2020**, *120*, 11028.
[39] A. M'barki, L. Bocquet, A. Stevenson, *Sci. Rep.* **2017**, *7*, 6017.
[40] L. del-Mazo-Barbara, M.-P. Ginebra, *J. Eur. Ceram. Soc.* **2021**, *41*, 18.
[41] T. Gao, G. J. Gillispie, J. S. Copus, A. K. PR, Y.-J. Seol, A. Atala, J. J. Yoo, S. J. Lee, *Biofabrication* **2018**, *10*, 034106.
[42] J. A. Lewis, J. E. Smay, J. Stuecker, J. Cesarano, *J. Am. Ceram. Soc.* **2006**, *89*, 3599.
[43] J.-Z. Liang, *Polym. Test.* **2002**, *21*, 927.
[44] M. Majid, E.-D. Hassan, A. Davoud, M. Saman, *Composites, Part B* **2011**, *42*, 2038.
[45] P.-C. Ma, N. A. Siddiqui, G. Marom, J.-K. Kim, *Composites, Part A* **2010**, *41*, 1345.
[46] M. Coffigniez, L. Gremillard, S. Balvay, J. Lachambre, J. Adrien, X. Boulnat, *Addit. Manuf.* **2021**, *39*, 101859.
[47] W. Wu, A. DeConinck, J. A. Lewis, *Adv. Mater.* **2011**, *23*, H178.
[48] Y. Sun, C. Peng, X. Wang, R. Wang, J. Yang, D. Zhang, *Powder Technol.* **2017**, *320*, 223.
[49] Q. Liu, W. Zhai, *ACS Appl. Mater. Interfaces* **2022**, *14*, 32196.
[50] Y. Li, B. Li, *Oxford Open Mater. Sci.* **2022**, *2*, itac008.
[51] B. Luo, Y. Wei, H. Chen, Z. Zhu, P. Fan, X. Xu, B. Xie, *ACS Appl. Mater. Interfaces* **2018**, *10*, 44796.
[52] A. Renteria, V. H. Balcorta, C. Marquez, A. A. Rodriguez, I. Renteria-Marquez, J. Regis, B. Wilburn, S. Patterson, D. Espalin, T.-L. (B). Tseng, Y. Lin, *Flex. Printed Electr.* **2022**, *7*, 15001.